# **MATERIALS SCIENCE**

# Accessing pluripotent materials through tempering of dynamic covalent polymer networks

Nicholas R. Boynton<sup>1</sup>, Joseph M. Dennis<sup>2</sup>, Neil D. Dolinski<sup>1</sup>, Charlie A. Lindberg<sup>1</sup>, Anthony P. Kotula<sup>3</sup>, Garrett L. Grocke<sup>1</sup>, Stephanie L. Vivod<sup>4</sup>, Joseph L. Lenhart<sup>2</sup>, Shrayesh N. Patel<sup>1,5</sup>\*, Stuart J. Rowan<sup>1,5,6</sup>\*

Pluripotency, which is defined as a system not fixed as to its developmental potentialities, is typically associated with biology and stem cells. Inspired by this concept, we report synthetic polymers that act as a single "pluripotent" feedstock and can be differentiated into a range of materials that exhibit different mechanical properties, from hard and brittle to soft and extensible. To achieve this, we have exploited dynamic covalent networks that contain labile, dynamic thia-Michael bonds, whose extent of bonding can be thermally modulated and retained through tempering, akin to the process used in metallurgy. In addition, we show that the shape memory behavior of these materials can be tailored through tempering and that these materials can be patterned to spatially control mechanical properties.

raditionally, polymer researchers have developed materials through iterative optimization of macromolecular structure [for example, (co)monomer type and sequence (1), architecture (2), and molecular weight (3)] to maximize specific performance metrics for a given application. This approach has worked well and led to the development of many different polymers that span a wide breadth of material properties. Inspired by pluripotent stem cells that have the ability to differentiate into various cell types (4-6), we have been interested in taking a different approach to polymer design by creating a pluripotent or "stem" polymer that has the ability to be differentiated into a range of different materials with disparate properties through exposure to an external stimuli. Such single-feedstock polymers could offer substantial advantages, for example, in resource-scarce areas (at sea, in space, or on the battlefield) where a single material could meet an evolving, complex set of demands and applications. Although chemical modification has been the main tool to alter polymer properties (7), a postsynthetic route to modify a single feedstock by using environmental or processing cues would be ideal for such resource-scarce areas. Perhaps the most accessible stimulus in most environments is heat, which has been used by materials scientists for centuries. For example, metallurgists use tempering-the isothermal heating of a material at a given tem-

example, metallurgists use tempering—the isothermal heating of a material at a given tem
1 Pritzker School of Molecular Engineering, University of Chicago, Chicago, IL 60637, USA. 2 Sciences of Extreme Materials Division, Polymers Branch, US DEVCOM Army Research Laboratory, Aberdeen Proving Ground, MD 21005, USA. 3 Materials Science and Engineering Division, National Institutes of Standards and Technology (NIST), Gaithersburg, MD 20899, USA. 4 NASA Glenn Research Center, Cleveland, OH 44135, USA. 5 Center for Molecular Engineering, Argonne National Laboratory,

University of Chicago, Chicago, IL 60637, USA. \*Corresponding author. Email: stuartrowan@uchicago.edu (S.J.R.); shrayesh@uchicago.edu (S.N.P.)

Lemont, IL 60439, USA. 6Department of Chemistry,

perature below a critical point (such as the melting point) before rapidly quenching (8, 9)to expand the application of steel from knives to structural beams. Inspired by this, we wondered whether it would be possible to design a single polymeric material that could access a range of mechanical properties by simply tempering that material at different temperatures. To design such a material it was proposed to leverage the following three criteria: (i) reconfigurable bonds that allow for bulk property manipulation, (ii) sensitivity to accessible and tunable stimuli conditions to allow access to a range of material properties, and (iii) an ability to retain properties within the operational temperature window of interest (Fig. 1A).

A wide range of reconfigurable dynamic bonds are accessible, which include supramolecular interactions (10, 11) and dynamic covalent chemistries (12-16) such as Diels-Alder (17), boronic acids (18), hindered ureas (19), urethanes (20), disulfides (21), and thiol-ene derivatives (22). Within polymeric materials, this array of dynamic chemistries has been exploited to alter the adaptive properties of the material and allow them to be used in applications such as nanogels (23), solid polymer electrolytes (24), and stress-adaptive suspensions (25). The reversibility of dynamic bonds under different environmental stimuli satisfies the first criterion. However, particular emphasis must be placed on materials that can be reconfigured at low processing temperatures (<100°C), without the use of a catalyst, to achieve practicality in resource-scarce areas. Previous work has shown that polymer networks that contain room-temperature dynamic thia-Michael (tM) bonds (26-30)—obtained through the catalyst-free reaction of a ditopic benzalcyanoacetate (BCA), end-capped triethylene glycol Michael acceptor with a tetrathiol cross-linker (Fig. 1B)-can be used to access films with robust mechanical properties on account of a dynamic reaction-induced phase separation (DRIPS) process (31, 32). The equilibrium stant ( $K_{\rm eq}$ ) of the thiol addition to the Michael acceptor can be controlled by the electronic nature of the BCA acceptor, which ranges from around 10  ${\rm M}^{-1}$  for electron-donating substituents (–OMe) to around 500  ${\rm M}^{-1}$  for electron-withdrawing substituents (–NO<sub>2</sub>). Given the temperature sensitivity of these relatively weak dynamic bonds, it was hypothesized that such networks may have the potential to be designed into temperable materials.

## Designing a pluripotent polymer

A ditopic Michael acceptor (1) with a pentaethylene glycol core was targeted to enhance the flexibility of the network, whereas the higherequilibrium constant p-nitro-BCA Michael acceptor was chosen to aid in maintaining mechanical robustness at elevated temperatures. Cross-linking 1 with pentaerythritol tetrakis(3-mercaptopropionate) (2) yielded the tM network ( $\mathbf{N}_x \mathbf{Y}$ , where x is the percentage of thiols from 2 and Y is the tempering temperature) films. A representative atomic force microscopy (AFM) image of an  $N_{100}60$  film is shown in Fig. 1C [where 60 is the temperature (°C) at which the film was isothermally heated (tempered) for at least 1 day before quenching with liquid nitrogen], in which the characteristic DRIPS microstructure of a continuous soft matrix with interspersed, globular hard domains can be observed. Differential scanning calorimetry (DSC) of  $N_{100}$  shows two thermal transitions (Fig. 1D, gray line), a low glass transition temperature  $(T_g)$ , and an upper thermal transition  $(T_{\rm LTT})$ . To be able to postsynthetically modify the materials, it is vital to have a tempering window that allows for tuning the number of dynamic bonds or cross-links formed in the film so that the mechanical properties can be influenced. For the BCA tM bond, estimations from solution-state <sup>1</sup>H nuclear magnetic resonance (NMR) spectroscopy experiments suggest a ≈40% decrease in the tM adducts (Fig. 1B) formed upon raising the temperature between the  $T_{\rm g}$  and  $T_{\rm UT}$  of this tM network (Fig. 1D), with substantially lower activation energy  $(E_a)$  for the bondformation reaction (45 kJ mol<sup>-1</sup>) than that for the bond-cleavage reaction (122 kJ mol<sup>-1</sup>) (fig. S3). It was hypothesized that after quenching to ambient temperatures, unwanted bond formation (bimolecular coupling) would be impeded by the increased viscosity, whereas unwanted bond breakage would be hindered by its relatively higher  $E_{av}$  stabilizing the tempered properties. This combination of (i) the presence of reconfigurable bonds, (ii) the thermal sensitivity of dynamic bonds within the tempering window, and (iii) the stabilization of the tempered properties at room temperature presents these tM networks as a prototypical system to explore tempering in a synthetic material.

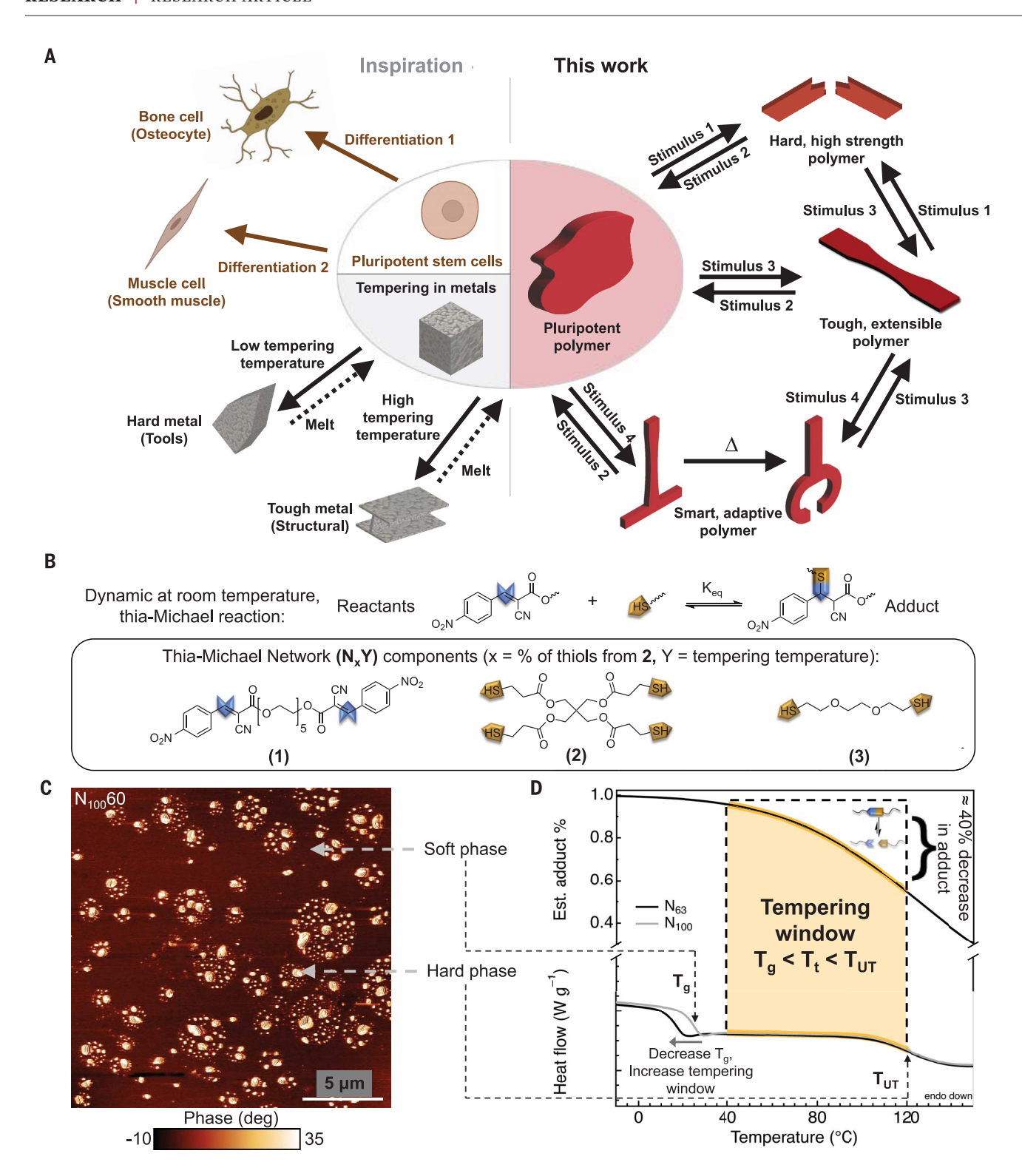


**Fig. 1. Pluripotent polymer design. (A)** Inspiration for the design of a pluripotent polymer comes from stem cells and the tempering of metals. **(B)** The dynamic tM bond consisting of a BCA-based Michael acceptor and thiol component, with the chemical structures of the tM network **(N)** components: a ditopic nitro-bearing Michael acceptor **(1)** (NMR characterization for all synthesized Michael acceptors in figs. S1 and S2), tetrathiol cross-linker **(2)**, and dithiol chain extender **(3)**, with the nomenclature  $\mathbf{N_xY}$ , where x is the percentage of thiols from **2** and Y is the tempering temperature. **(C)** Representative AFM phase micrograph of  $\mathbf{N_{100}60}$  showing a DRIPS microstructure with globular hard domains (light) interspersed in a soft matrix (dark). **(D)** Defining

the tempering temperature window ( $T_{\rm t}$ ) for these dynamic networks. (Top) The estimated adduct percentage as calculated from solution-state  $^{1}{\rm H}$  NMR experiments (figs. S3 and S4) highlighting a ~40% decrease in adduct percentage from 45° to 120°C (the tempering window). (Bottom) A DSC thermogram of  $N_{100}$  (gray curve) that shows the presence of two thermal transitions: a lower glass transition temperature ( $T_{\rm UT}$ ) corresponding to the hard phase of the DRIPS microstructure. The tempering window is defined as the temperature range between  $T_{\rm g}$  and  $T_{\rm UT}$ . The tempering window can be expanded by decreasing the  $T_{\rm g}$  through introduction of the dithiol 3 during the network synthesis, as shown, for example, for the  $N_{\rm 63}$  film (black curve).

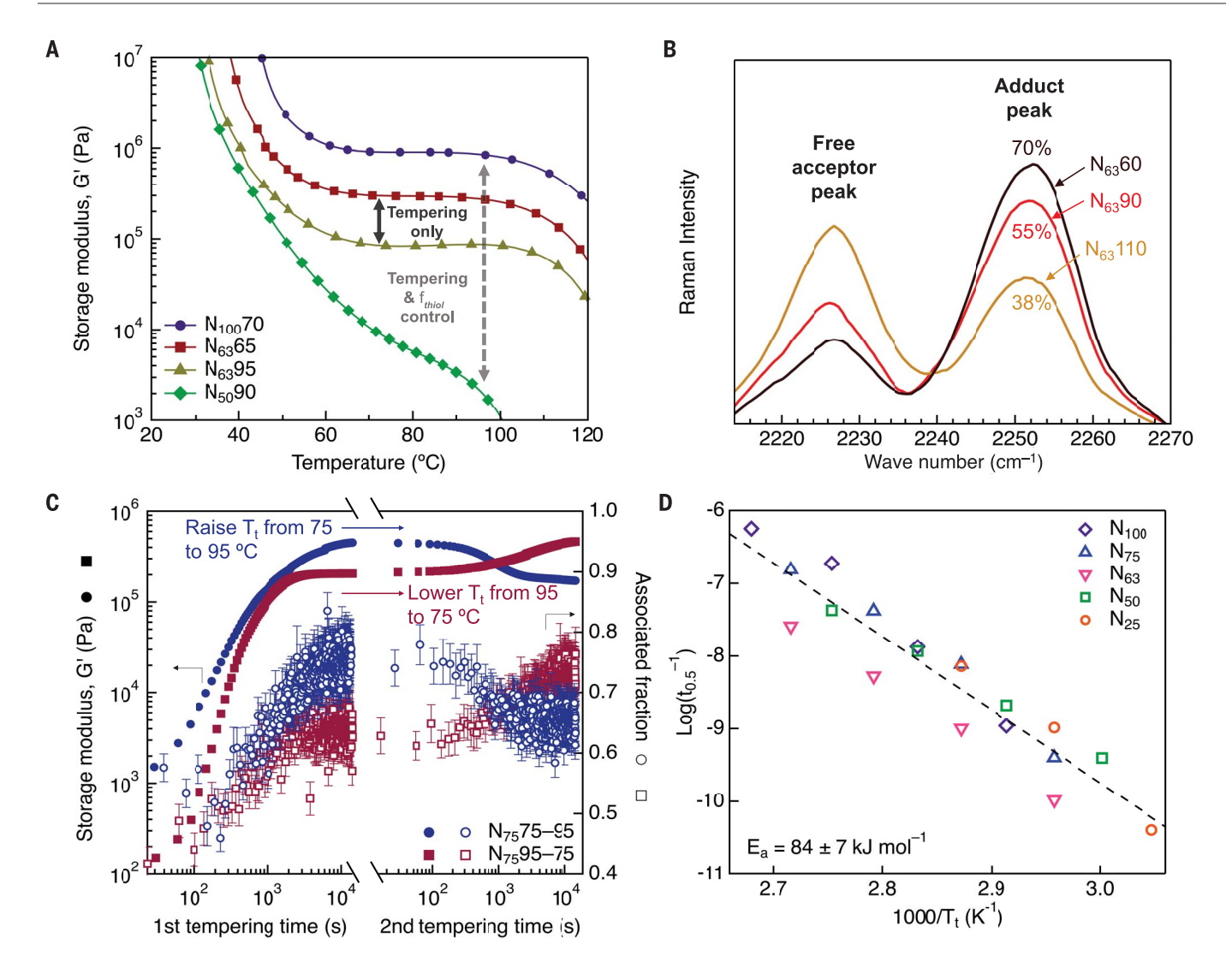


**Fig. 2. Tempering process in N**<sub>x</sub>**Y**. (**A**) Temperature-dependent storage modulus, G' for  $\mathbf{N}_{100}70$ ,  $\mathbf{N}_{63}65$ ,  $\mathbf{N}_{63}95$ , and  $\mathbf{N}_{50}90$  showing that both  $f_{\text{thiol}}$  and  $T_{\text{t}}$  affect G'. For the  $\mathbf{N}_{63}$ **Y** film, there is a 3.5-fold increase in G' (at 80°C) from  $\mathbf{N}_{63}$ **95** (84 kPa) to  $\mathbf{N}_{63}$ **65** (295 kPa) with the lower  $T_{\text{t}}$ . There is also a minor shift in  $T_g$ , with  $\mathbf{N}_{63}$ **95** (35°C) having a 4°C lower  $T_g$  than  $\mathbf{N}_{63}$ **65** (39°C). (**B**) Room-temperature partial Raman spectra of  $\mathbf{N}_{63}$  films tempered at various  $T_{\text{t}}$ , with the nitrile stretch of the free acceptor peak at 2227 cm<sup>-1</sup> and the nitrile stretch of the adduct peak at 2253 cm<sup>-1</sup>. (**C**) Two-step rheo-Raman experiment in which films of  $\mathbf{N}_{75}$ **95–75** (red squares) and  $\mathbf{N}_{75}$ **75–95** (blue circles) were first isothermally held at 145°C for 15 min to erase

history before rapid cooling to the specified temperature. Upon reaching  $T_{\rm t}$ , the evolution of G' and rise in associated fraction demonstrates that increasing associated fraction of tM bonds (determined from Raman data) leads to increased G', and that the process is reversible. Error bars in the associated fraction represent the standard error from the uncertainty in fitting of the two nitrile stretch peaks (a more detailed discussion is available in fig. S10). (**D**) Arrhenius plot of  $t_{0.5}$  values from normalized growth curves against  $T_{\rm t}$  for all  $N_{\rm x}Y$  films with an activation energy  $E_{\rm a}$  of  $84 \pm 7~{\rm kJ~mol}^{-1}$ , which is attributed to a combination of dynamic bond exchange and segmental mobility of the network.

To lower the  $T_{\rm g}$  and expand the tempering window, a series of materials with varying network compositions were prepared in which 1 was combined with a mixture of tetrathiol (2) and dithiol, 2,2'-(ethylenedioxy)diethanethiol (3) (in ratios of 100:0, 75:25, 63:37, 50:50, 25:75, and 0:100, respectively, based on the percentage of thiols from that particular component) at a 1:1 stoichiometric ratio of [double bond]:[thiol]. Thermal gravimetric analysis (TGA) demonstrated that all films were dry and had decomposition temperatures ranging from 215° to 262°C (fig. S5). DSC and shear rheometry (figs. S6 and S7) confirmed two characteristic ther-

mal transitions at all network compositions and identified an increase in the width of the tempering window (Fig. 1D, black curve), with decreasing average functionality of the thiol components ( $f_{\text{thiol}}$ , ranging from  $f_{\text{thiol}}$  of 4 for  $\mathbf{N_{100}}$  to  $f_{\text{thiol}}$  of 2 for  $\mathbf{N_0}$ ). Each  $\mathbf{N_x}$  was tempered by using a tempering temperature ( $T_{\text{t}}$ ) within the tempering window, whereafter the thermomechanical properties were measured with shear rheometry (Fig. 2A and fig. S7). For films with at least 50% of the tetrathiol  $\mathbf{2}$ , both  $T_{\text{g}}$  and the plateau storage modulus (G') increased with decreasing  $T_{\text{b}}$  with the difference in G' retained throughout the tempering win-

dow. Within a single network composition, an increase of  $3.5\times$  in G' and  $5^{\circ}\mathrm{C}$  in  $T_{\mathrm{g}}$  was realized by changing  $T_{\mathrm{t}}$  from 95° to 65°C. By manipulating the formulation with  $f_{\mathrm{thiol}}$ , a two-order-of-magnitude change in the thermomechanical properties of the  $\mathbf{N}_x \mathbf{Y}$  films can be accessed. On account of its room-temperature operational window and large variation in G',  $\mathbf{N}_{63}$  was chosen for further investigation of the underlying mechanism of tempering in the  $\mathbf{N}_x \mathbf{Y}$  films.

The changes in the thermomechanical properties (such as moduli and  $T_{\rm g}$ ) could be governed by the underlying DRIPS microstructure,

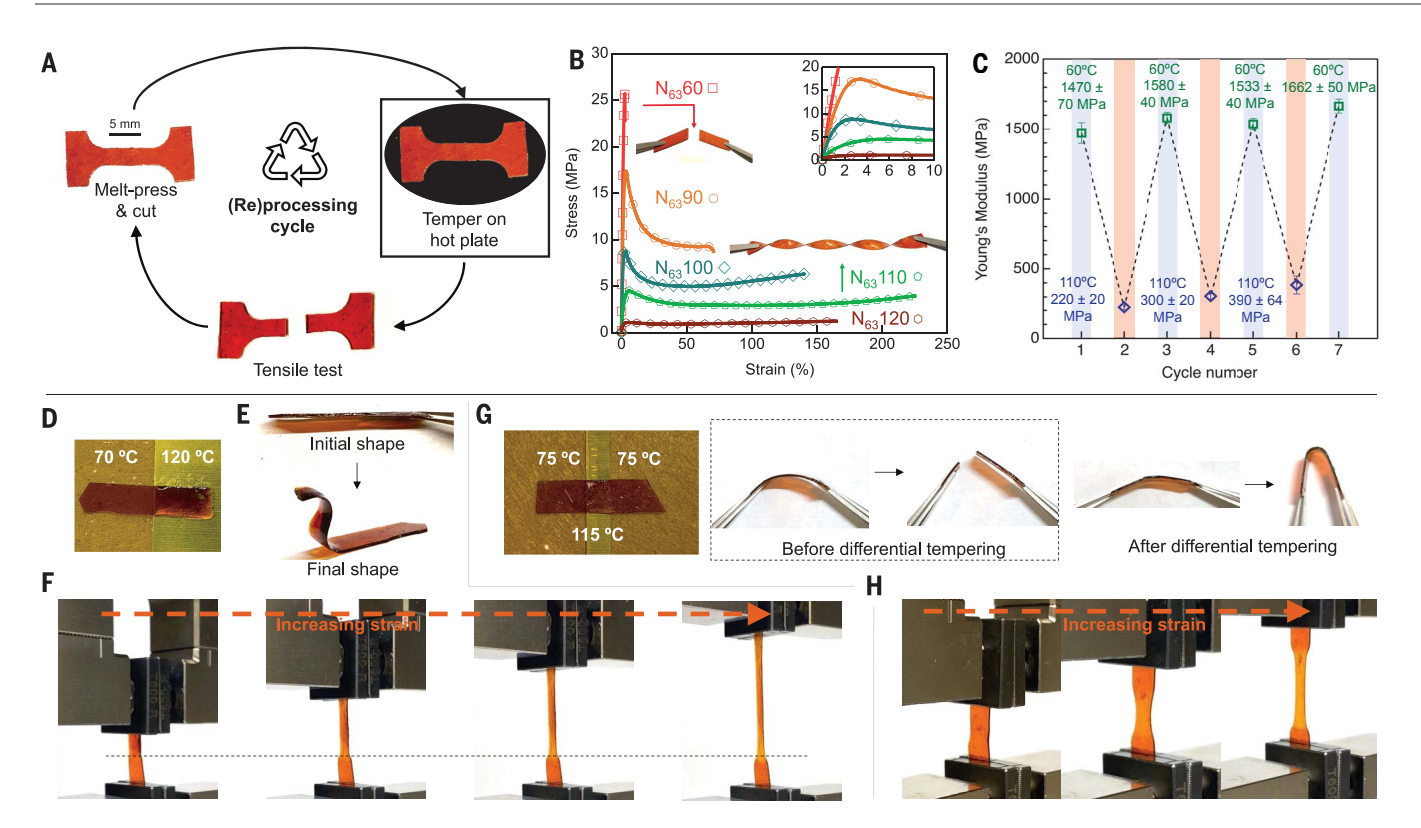


**Fig. 3. Reprocessability of N**<sub>x</sub>**Y**. **(A)** Schematic of the processing-reprocessing cycle for a dogbone specimen of a **N**<sub>63</sub>**Y**. **(B)** Representative stress-strain curves (at room temperature) of **N**<sub>63</sub>**60** (n = 5; red squares), **N**<sub>63</sub>**90** (n = 9; orange circles), **N**<sub>63</sub>**100** (n = 5; blue rhombuses), **N**<sub>63</sub>**110** (n = 4; green pentagons), and **N**<sub>63</sub>**120** (n = 6; brown hexagons) films with a strain rate of 25% min<sup>-1</sup>. Dogbone specimens were tempered for <24 hours under inert atmosphere and quenched on a cold, metal block before testing (SM materials and methods). **(C)** Young's modulus versus recycling experiments showing the ability of the film to be reprogrammed between **N**<sub>63</sub>**60** [with n = 5 (cycle 1), 6 (cycle 3), 4 (cycle 5), and 5 (cycle 7)] and **N**<sub>63</sub>**110** [with n = 7 (cycle 2), 6 (cycle 4), and 3 (cycle 6)]

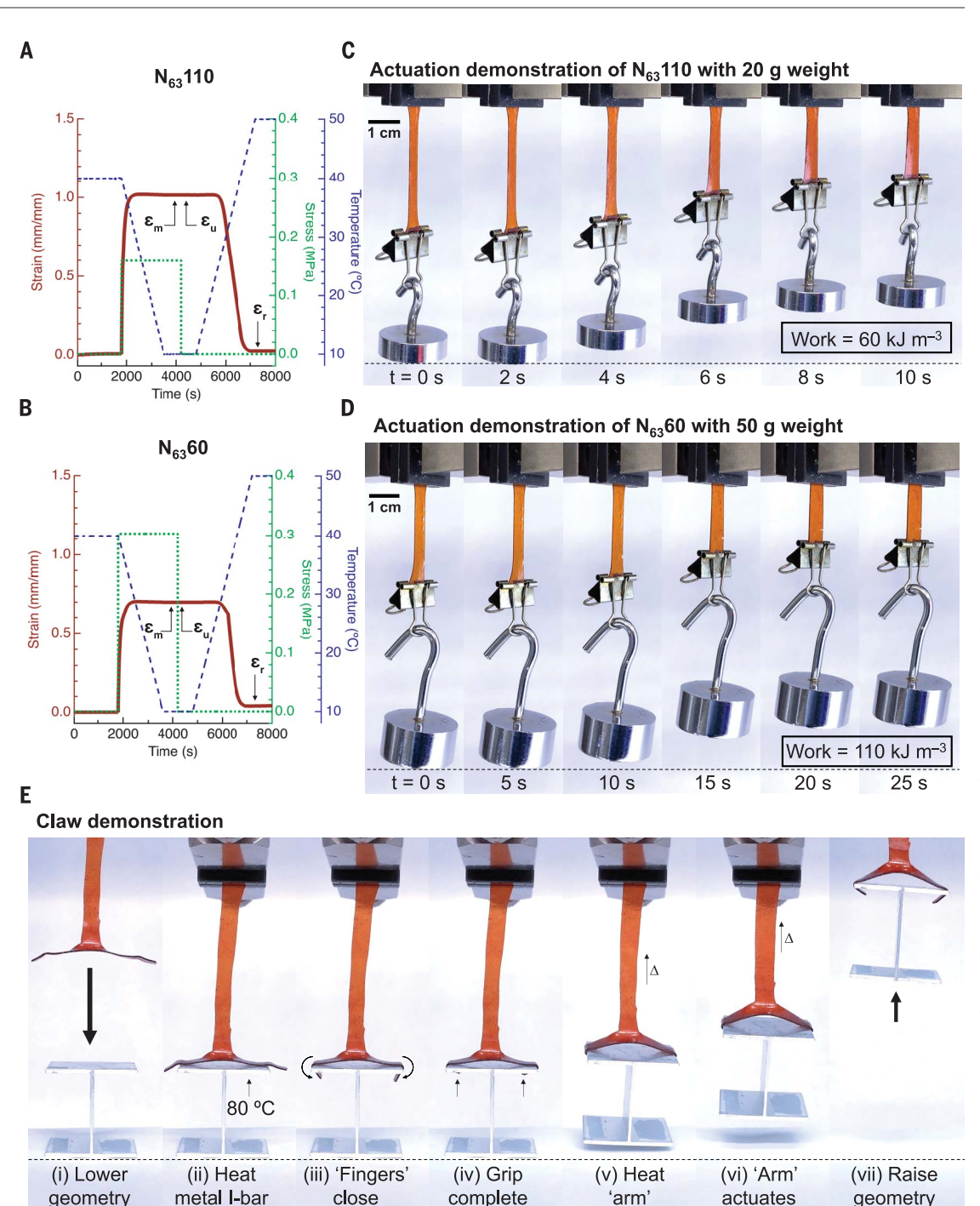
(full stress-strain curves are shown in fig. S20). (**D**) Picture of AB differential tempering stage with  $N_{63}$  film. (**E**) Image of  $N_{63}$  film after differential tempering, before and after applying stress (movie S4). (**F**) Images of AB differentially tempered  $N_{63}$  film during tensile testing with strain visible in the soft, extensible section of the film but not in the rigid section (movie S5). (**G**) Picture of ABA differential tempering stage with  $N_{63}$  film. Before differential tempering, the film experienced brittle failure upon bending, whereas it was able to bend without failure after differential tempering (movie S6). (**H**) Images of ABA differentially tempered film progressing from bar specimen before application of strain to dogbone-like specimen after the strain was applied (movie S7).

changes in the amount of dynamic bond formed within the network, or a combination of both. Although AFM confirmed a decrease in the hard phase with decreasing  $f_{\rm thiol}$  (fig. S8), no clear trends were observed when a film (of set  $f_{\text{thiol}}$ ) was tempered at different  $T_{\text{t}}$  [a detailed explanation of tempering for AFM samples is available in the supplementary materials (SM), materials and methods], suggesting that the amount of hard phase is not the primary mechanism that drives the substantial changes in mechanical properties with tempering conditions. This is in stark contrast to previous results in which the cooling rate through the  $T_{\rm LIT}$  resulted in changes to nucleation and growth of the hard phase that led to differences in final mechanical properties (31). Raman spectroscopy can assess the amount of Michael adduct (2257 cm<sup>-1</sup>) and unreacted BCA moieties (2227 cm<sup>-1</sup>) present in the films after the tempering process by monitoring the shift in the nitrile stretch upon bonding. Part of the room-temperature Raman spectra of a N<sub>63</sub> film after it was tempered at three different

 $T_{\rm t}$  is shown in Fig. 2B. The data show that the amount of adduct in the film is highly dependent on the  $T_t$ . Higher  $T_t$  results in a reduction in the amount of adduct and therefore a network with lower cross-linking density (fig. S9). Such coupling of the  $T_t$  and crosslinking density correlates well with decreasing stiffness in the dynamic network films tempered at high  $T_{\rm t}$ . To further support this hypothesis, we carried out rheo-Raman experiments (33) to probe the time-temperature dependence of the film's tM equilibrium and mechanical properties during the tempering process. In Fig. 2C, we overlay the storage moduli and fraction of adduct as a function of time and  $T_{\rm t}$  for a representative material  $N_{75}$  $(N_{63}$  is shown in fig. S10). As illustrated, the growth in G' of  $N_{75}$  at 95°C (Fig. 2C, red curve) was concomitant with an increase in the amount of tM adducts formed. When the  $T_t$  was then lowered to 75°C, there was a distinct rise in both G' and the amount of tM adduct in the film. If a film is initially heated at 75°C, the equilibrium modulus and tM adduct fraction is the same as that in the film tempered at 95°C followed by 75°C (Fig. 2C, blue curve). Heating the 75°C tempered film to 95°C results in a gradual decrease in both modulus and tM adduct formed.

As shown by the rheo-Raman data, the combination of tempering with these tM dynamic bonds leads to materials with reconfigurable cross-linking density and controllable mechanical properties, independent of the tempering pathway. Time-resolved shear rheometry was used to monitor the evolution of G' with time for the films with varying network compositions (fig. S11), further confirming that tempering at lower  $T_t$  resulted in a higher, equilibrated G' plateau, driven by an increase in adduct formation. After normalization of G'. the time required to reach the halfway point  $(t_{0.5})$  (fig. S12) in the growth curves could be collapsed into a simple Arrhenius relationship (Fig. 2D), suggesting that growth of G' followed a similar evolution process, independent of network composition, with an activation energy of 84  $\pm$  7 kJ mol<sup>-1</sup> for the  $N_xY$  films. Because

Fig. 4. Adaptive, temperable materials. (A and B) Thermomechanical shape memory curves for (A)  $N_{63}110$  and (B)  $N_{63}60$ obtained from dynamic mechanical analysis (DMA) experiments. (C) Shape memory actuation demonstration for N<sub>63</sub>110 with a 20-g weight attached (movie S8). (D) Shape memory actuation demonstration for N<sub>63</sub>60 with a 50-g weight attached (movie S9). (E) Images of the shape memory "claw" demonstration for  $N_{63}100$  in which (i) the geometry is lowered until the claw contacts the I-bar, (ii) the fingers of the claw then contact the heated I-bar (≈ 80°C). which (iii) stimulates the fingers of the claw to spontaneously close around the I-bar. (iv) Once the grip of the fingers is complete, (v) the "arm" of the claw is heated (≈ 60°C) to (vi) initiate actuation of the arm, which removes the I-bar from contact with the ground. After this, (vii) the geometry is raised to demonstrate successful grip of the I-bar by the claw (fig. S29 and movie S10).



changes in adduct fraction and segmental mobility primarily drive the changes in mechanical properties, it is unsurprising that all materials follow a similar G' evolution process. However, this measured activation energy does not correlate precisely to that of the dynamic bond itself in  $\mathbf{N}_x Y$ , either in bond formation (45 kJ mol<sup>-1</sup>) or bond cleavage (around 122 kJ mol<sup>-1</sup>) (fig. S3). The tempering process was further generalized to tM networks that contain hydrogen-substituted Michael acceptors ( $\mathbf{H}_x Y$ ) (fig. S13) to ensure that temper-

ing was not substituent-dependent and yielded a similar  $E_a$  of 89  $\pm$  2 kJ mol<sup>-1</sup>.

# Reforging plastic

One of the key advantages of dynamic polymer networks over traditional covalent networks is their ability to be reprocessed and recover their original mechanical properties (34). Although reprocessing does allow recovery of a single mechanical performance, tempering has the added benefit of being able to define or redefine the material properties across a range

of common polymer mechanical properties through control of Young's modulus, E, and strain at break  $(\epsilon_b)$  (fig. S14). Programming or reprogramming dogbone specimens of  $\mathbf{N_{63}}$  at various  $T_t$  illustrates the tailorability and reliability of this method to achieve different, repeatable mechanical performance from a single material after tempering for <24 hours (with the exception of  $\mathbf{N_{63}60}$ , which was tempered for 48 hours) with a simple quenching step on a cold, metal block (Fig. 3A, fig. S15, table S1, and SM materials and methods). Although all

samples were tempered under an inert atmosphere to prevent unwanted side reactions, there was no evidence of disulfide formation when tempering under open, ambient conditions for 9 days, suggesting that tempering could be achieved without inert conditions (fig. S16). Programming with  $T_t$  of 60°C, 70°C (fig. S17), 90°C, 100°C, 110°C, and 120°C resulted in a spectrum of room-temperature properties, ranging from brittle thermoset (E = 1520  $\pm$ 60 MPa,  $\varepsilon_b$  = 11 ± 5%) (Fig. 3B, red curve) to tough thermoplastic ( $E = 670 \pm 84$  MPa,  $\varepsilon_{\rm b} =$  $130 \pm 30\%$ ) (Fig. 3B, blue curve) and soft, extensible polymer ( $E = 210 \pm 20$  MPa,  $\varepsilon_b = 250 \pm$ 14%) (Fig. 3B, green curve), respectively. This property range enables this single feedstock to be used in very different applications (fig. S18). For example, the material tempered at 60°C  $(N_{63}60)$  can be used in make utensils, such as a spoon that can scoop peanut butter or a fork that can pick up cheese (fig. S18, A to E, and movies S1 and S2). Tempering at 110°C results in a material ( $N_{63}110$ ) that can now act as an adhesive with body temperature and pressure (fig. S18F and movie S3). N<sub>63</sub>60 does not exhibit adhesive behavior under the same bonding conditions (fig. S18G). Further investigation also demonstrated that tempering could control E in the lower- $T_g$  ( $\approx 0$ °C) materials that contain a mixture of  $\mathbf{N}/\mathbf{H}_{r}\mathbf{Y}$  (fig. S19) and that this could be achieved outside a glovebox. Beyond programming across this range of properties at room temperature, the ability to cycle (or recycle) between  $N_{63}60$  (E = 1470 ± 70 MPa on first cycle to  $E = 1660 \pm 50$  MPa after six reprocessing cycles) and  $N_{63}110$  (E = 220 ± 20 MPa on first cycle to  $E = 390 \pm 64$  MPa after four reprocessing cycles) is illustrated in Fig. 3C, with the Young's modulus being generally within error during the processing cycles (fig. S20). Furthermore, mechanical aging studies (SM materials and methods) confirmed that the moduli could be effectively retained for more than a month in both  $N_{63}60$  (loss of ~1.1 MPa day<sup>-1</sup>) and **N<sub>63</sub>110** (gain of ~2.2 MPa day<sup>-1</sup>) (fig. S21). These experiments highlight the ability to temper-in mechanical properties at a specific operating temperature (room temperature for this study), easily switch between these properties without any chemical modification, and retain those tempered-in properties for more than a month.

To expand the type of behavior achievable in a material, metallurgists have commonly used differential tempering to spatially control mechanical properties (for example, in swords with sharp edges and toughened spines). The ability to spatially control a film's mechanical properties has been an emergent area of study in polymer design and synthesis (35, 36). Within additive manufacturing (37-39), this technique is used to access different multimaterial designs previously limited to biological materials (40). Although advanced strategies have

addressed early concerns about poor interfaces between materials (41), limitations still exist in recycling or reprogramming the materials after they are formed. The tempering of dynamic covalent networks has the potential to enable access to interesting multimaterial or mechanically graded designs in recyclable  $\mathbf{N}_x \mathbf{Y}$  materials. As a first demonstration, we prepared a N<sub>63</sub>60 film to create a hard, brittle plastic with high strength and low toughness. Next, we placed the film onto a heated block composed of half aluminum and half polyimide fiber insulation (Fig. 3D and SM materials and methods) to locally temper only the film exposed to the aluminum substrate, as confirmed with an infrared (IR) camera (fig. S22). After tempering, the film showed preferential deformation in the "softer" region processed at a higher  $T_t$  (Fig. 3E, fig. S23, and movie S4). Additionally, the differentially tempered bar was loaded into a mechanical load frame at room temperature and strained to failure. On application of strain, the extensible, high- $T_t$ network preferentially deformed under the low applied stresses, whereas the other half had no observable deformation occur (Fig. 3F and movie S5). For increased complexity, an ABA system was prepared by means of a lowhigh-low spatial tempering process (Fig. 3G and SM materials and methods), as confirmed with an IR camera image (fig. S24), imparting a hinge-like response under bending in contrast to the brittle failure of the untempered material (movie S6). The preferential deformation was further illustrated on the hinge-like sample by using a mechanical load frame and nominal strain rate of 25% min<sup>-1</sup>. As expected, the material deformed in the region tempered at higher  $T_t$ , leading to a local ductile failure away from the interface (Fig. 3H and movie S7). A more complex "S" shape was also differentially tempered in an N<sub>63</sub> film and could be visualized upon strain (fig. S25). From these demonstrations, differential tempering of a single film can be used to access spatially controlled mechanical properties without the need for complex welding or adhesion of disparate materials and could be further expanded through more complex patterning techniques in future studies (42). The shape of the AB system could be recovered through light heating (rubbing with fingertips), which motivated further investigation through cyclic loadingunloading experiments (SM materials and methods). Through these experiments, the yielding behavior could be recovered through both time and temperature, suggesting an ability to minimize material performance degradation from plastic deformation (fig. S26).

# Tempering-in the material's stimuli-responsive properties

The ability to control mechanical properties is an important aspect of demonstrating temperable materials; however, expanding this control to tailoring the material's stimuli-responsive nature gives access to an even broader range of applications. Because related DRIPS networks have been shown to exhibit shape memory behavior (31), it was of interest to see whether tempering could be used to alter this responsive property. Tempering N<sub>63</sub> at 110°C (N<sub>63</sub>110) showed an ideal fixing ratio [maximum strain (Em) divided by unloading strain  $(\epsilon_u)$ ] of 1.0 and excellent shape recovery (94%) after reaching an  $\epsilon_m$  of 100% upon loading of 0.16 MPa (Fig. 4A and SM materials and methods). By contrast, N<sub>63</sub> tempered at 60°C  $(N_{63}60)$  exhibited a 30% reduction in  $\varepsilon_m$  relative to  $N_{63}110$ , despite an almost doubling of the force (0.30 MPa) applied during the shape-fixing process (Fig. 4B). At the service temperatures of 30° and 60°C, both N<sub>63</sub>60 (0.02% hour<sup>-1</sup> and 0.11% hour<sup>-1</sup>, respectively) and N<sub>63</sub>110 (0.10% hour<sup>-1</sup> and 0.52% hour<sup>-1</sup>, respectively) showed minimal creep (fig. S27). To further demonstrate the contrast in actuation between materials tempered at different  $T_t$ ,  $N_{63}110$  and  $N_{63}60$  were extended to 300 and 220% strain, respectively (SM materials and methods). Upon heating,  $N_{63}110$  could linearly lift a 20-g weight (work = 60 kJ m<sup>-3</sup>) (Fig. 4C, fig. S28, and movie S8), whereas the N<sub>63</sub>60 was able to linearly lift a 50-g weight over a smaller displacement (work = 110 kJ m<sup>-3</sup>) (Fig. 4D and movie S9).

As a final proof of concept of these materials' shape memory and linear actuation capabilities, a "T" shape was cut from a film of N<sub>62</sub> and folded into a claw-like shape around a metal I-bar before being tempered at 100°C for 1 hour (fig. S29). After deformation, the claw was fixed to tensile grips and slowly lowered to a heated metal I-bar, where the "fingers" of the claw grasped the I-bar (Fig. 4E and movie S10). Upon heating, the arm linearly actuated and lifted the I-bar from the ground. As the tensile grips were raised, the claw maintained control of the I-bar. Thus, materials not only can be made to have passive properties of interest through control of tempering but can also be rationally designed to create adaptive, multifunctional materials.

We describe a strategy to design dynamic covalent polymer network materials that can be easily differentiated through tempering and reprocessed to exhibit a wide range of material properties. These materials, which exploit a synergistic relationship between dynamic networks and phase separation, show a range of room-temperature properties from brittle and glassy (E = 1520  $\pm$  60 MPa,  $\varepsilon_{\rm b}$  = 11  $\pm$  0.4%) to soft and extensible ( $E = 210 \pm 20$  MPa,  $\varepsilon_b =$  $250 \pm 14\%$ ) with a simple change in tempering temperature, without requiring any external chemical modification or additives. These materials also exhibit shape-memory properties, and careful control of the material form

factor and programming enables control of the material response that could be used in soft robotics applications.

### **REFERENCES AND NOTES**

- 1. C. M. Bates, F. S. Bates, Macromolecules 50, 3-22 (2017).
- G. Polymeropoulos et al., Macromolecules 50, 1253-1290 (2017)
- L. J. Fetters, D. J. Lohse, D. Richter, T. A. Witten, A. Zirkel, Macromolecules 27, 4639-4647 (1994).
- J. A. Thomson et al., Science 282, 1145-1147 (1998)
- D. A. Robinton, G. Q. Daley, Nature 481, 295-305 (2012).
- K. Takahashi, S. Yamanaka, Cell 126, 663-676 (2006).
- E. Blasco, M. B. Sims, A. S. Goldmann, B. S. Sumerlin,
- C. Barner-Kowollik, Macromolecules 50, 5215-5252 (2017). G. R. Speich, W. C. Leslie, Metall. Trans. 3, 1043-1054 (1972).
- L. J. E. Hofer, E. M. Cohn, Nature 167, 977–978 (1951).
- 10. J.-M. Lehn, Chem. Soc. Rev. 36, 151-160 (2007).
- T. Aida, E. W. Meijer, S. I. Stupp, Science 335, 813-817 (2012).
- 12. S. J. Rowan, S. J. Cantrill, G. R. L. Cousins, J. K. M. Sanders, J. F. Stoddart, Angew. Chem. Int. Ed. 41, 898-952 (2002).
- 13. R. J. Woitecki, M. A. Meador, S. J. Rowan, Nat. Mater. 10, 14-27 (2011)
- 14. M. Podgórski et al., Adv. Mater. 32, e1906876 (2020).
- 15. J. M. Winne, L. Leibler, F. E. Du Prez, Polym. Chem. 10, 6091-6108 (2019).
- 16. V. Zhang, B. Kang, J. V. Accardo, J. A. Kalow, J. Am. Chem. Soc. 144, 22358-22377 (2022).
- 17. B. Zhang et al., Polym. Chem. 6, 7368-7372 (2015).
- 18. C. C. Deng, W. L. A. Brooks, K. A. Abboud, B. S. Sumerlin, ACS Macro Lett. 4, 220-224 (2015).
- 19. M. A. Bin Rusayyis, J. M. Torkelson, ACS Macro Lett. 11, 568-574 (2022).
- 20. J. L. Swartz, D. T. Sheppard, G. Haugstad, W. R. Dichtel, Macromolecules 54, 11126-11133 (2021).
- 21. R. Kato et al., ACS Macro Lett. 9, 500-506 (2020)
- 22. J. S. A. Ishibashi, J. A. Kalow, ACS Macro Lett. 7, 482-486
- 23. G. Gao et al., ACS Macro Lett. 9, 713-719 (2020).
- 24. B. B. Jing, C. M. Evans, J. Am. Chem. Soc. 141, 18932-18937 (2019).
- 25. G. L. Jackson et al., Macromolecules 55, 6453-6461
- 26. Y. Zhong, Y. Xu, E. V. Anslyn, Eur. J. Org. Chem. 2013, 5017-5021 (2013).
- 27. T. M. FitzSimons, F. Oentoro, T. V. Shanbhag, E. V. Anslyn, A M Rosales Macromolecules 53 3738-3746 (2020)

- 28. T. M. FitzSimons, E. V. Anslyn, A. M. Rosales, ACS Polym. Au 2, 129-136 (2022).
- 29 I M Serafimova et al. Nat. Chem. Biol. 8, 471-476 (2012).
- 30. E. H. Krenske, R. C. Petter, K. N. Houk, J. Org. Chem. 81, 11726-11733 (2016).
- 31. K. M. Herbert et al., Chem. Sci. 11, 5028-5036 (2020).
- 32. K. M. Herbert et al., ACS Appl. Mater. Interfaces 13, 27471-27480 (2021)
- 33. A. P. Kotula et al., Rev. Sci. Instrum. 87, 105105 (2016).
- 34. G. M. Scheutz, J. J. Lessard, M. B. Sims, B. S. Sumerlin, J. Am. Chem. Soc. 141, 16181-16196 (2019)
- 35. A. K. Rylski et al., Science 378, 211-215 (2022).
- 36. M. J. Allen et al., Adv. Mater. 35, e2210208 (2023).
- 37. G. I. Peterson et al., ACS Appl. Mater. Interfaces 8, 29037-29043 (2016).
- 38. N. D. Dolinski et al., Adv. Mater. 30, e1800364 (2018).
- 39. N. D. Dolinski et al., ACS Appl. Mater. Interfaces 13,
- 22065-22072 (2021).
- 40. A. R. Studart, Chem. Soc. Rev. 45, 359-376 (2016). 41. J. R. Tumbleston et al., Science 347, 1349-1352 (2015).
- 42. Z. Nie, E. Kumacheva, Nat. Mater. 7, 277-290 (2008).

#### **ACKNOWLEDGMENTS**

Parts of this work were carried out at the Soft Matter Characterization Facility and the Materials Research Science and Engineering Center (MRSEC NSF DMR 2011854) at the University of Chicago. The authors thank A. Crolais for high-resolution mass spectrometry (HRMS) of 1. The authors thank P. Griffin, J. Jureller, and T. Jorgenson for insightful advice on instrumentation. The authors thank S. Hossainy for his help designing Fig. 1 using BioRender.com. The authors also thank G. Solymosy and T. Hagan for their help with chemical synthesis during revisions. The authors also thank B. Lewis and G. Shekhawat for their help with AFM during revisions, who made use of the SPID facility of Northwestern University's NUANCE Center, which has received support from the SHyNE Resource (NSF ECCS-2025633), the IIN, and Northwestern's MRSEC program (NSF DMR-2308691). The views and conclusions contained in this document are those of the authors and should not be interpreted as representing the official policies, either expressed or implied, of the Army Research Laboratory or the US government. The US government is authorized to reproduce and distribute reprints for government purposes notwithstanding any copyright notation herein. Certain commercial equipment, instruments, or materials are identified in this paper to specify the experimental procedure adequately. Such identification is not intended to imply

recommendation or endorsement by the National Institute of Standards and Technology, nor is it intended to imply that the materials or equipment identified are necessarily the best available for the purpose. Funding: This work was supported by National Science Foundation under award DMR-2104694 and by the University of Chicago Materials Research Science and Engineering Center, which is funded by the National Science Foundation under award DMR-2011854. N.R.B. was supported by a NASA Space Technology Graduate Research Opportunity at the NASA Glenn Research Center. J.M.D. was sponsored by the Army Research Laboratory under Cooperative Agreement W911NF-20-2-0044, and N.D.D. was supported in part by the NIST Center for Hierarchical Materials Design, 60NANB15D077. This work was also supported by a National Science Foundation grant, DMR-2104694 (S.J.R.); NASA Space Technology Graduate Research Opportunity, 80NSSC21K1296 (N.R.B.); Army Research Laboratory Cooperative Agreement, W911NF-20-2-0044 (J.M.D. and J.L.L.): NIST Center for Hierarchical Materials Design, 60NANB15D077 (N.D.D.); and a National Science Foundation grant, DMR-2011854 (S.J.R. and C.A.L.). Author contributions: Conceptualization: N.R.B., J.M.D., N.D.D., S.N.P., and S.J.R. Methodology: N.R.B., J.M.D., N.D.D., C.A.L., A.P.K., G.L.G., S.L.V., S.N.P., and S.J.R. Investigation: N.R.B., J.M.D., N.D.D., C.A.L., A.P.K., and G.L.G. Visualization: N.R.B. and N.D.D. Funding acquisition: J.L.L. and S.J.R. Project administration: S.L.V., S.N.P., and S.J.R. Supervision: J.M.D., N.D.D., S.L.V., J.L.L., S.N.P., and S.J.R. Writing - original draft: N.R.B., J.M.D., N.D.D., and S.J.R. Writing review and editing: N.R.B., J.M.D., N.D.D., C.A.L., A.P.K., G.L.G., S.L.V., J.L.L., S.N.P., and S.J.R. Competing interests: The authors declare they have no competing interests. Data and materials availability: All data are available in the main text or the supplementary materials. License information: Copyright © 2024 the authors, some rights reserved; exclusive licensee American Association for the Advancement of Science. No claim to original US government works. https://www.science.org/about/sciencelicenses-iournal-article-reuse

#### SUPPLEMENTARY MATERIALS

science.org/doi/10.1126/science.adi5009 Materials and Methods Supplementary Text Figs. S1 to S29 Table S1 References (43-48) Movies S1 to S10

Submitted 29 April 2023; accepted 1 December 2023 10.1126/science.adi5009